

PACS numbers: 42.55.Wd; 42.65.Ky; 42.70.Mp
DOI: 10.1070/QE2007v037n07ABEH013305

Peculiarites of second harmonic generation of radiation from a pulsed ytterbium-doped fibre laser in $KTiOPO_4$ crystals

B.L. Davydov, A.A. Krylov

Abstract. **Second harmonic generation of radiation from a high-power fibre Yb^{3+} laser is studied upon sf – f phase matching near the *X* axis of the KTP crystal ($KTiOPO_4$). The temperature dependence of the phase-matching wavelength as well as its spectral, angular and temperature tuning characteristics of the second harmonic generator are experimentally measured. It is found that the increase in the average output power of the second harmonic in a single crystal is limited, first of all, by the thermal self-focusing of radiation caused by the absorption of radiation from the second harmonic, whose threshold decreases with increasing the crystal temperature. When the two-channel scheme is used, the maximum stable $\sim$ 4-W output power of the second harmonic is obtained in two tandem KTP crystals.**

Keywords: *second harmonic generation, KTP crystals, fibre laser*.

1. Introduction

The extensive development of fibre lasers has lead to the fabrication of lasers emitting average powers in a broad range – from milliwatts to several tens of kilowatts [1]. The advantages of fibre lasers are their ability to emit both multimode and single-mode beams in a wide spectral range, ultimate efficiency, compactness and high reliability. As a result, fibre lasers are widely used in fibreoptic communication, polygraphy, medicine as well as in laser welding and cutting of materials [1]. High average and pulsed powers have made these lasers promising for applications in processes of nonlinear frequency conversion, in particular, to generate second and third harmonics of a high average power [2, 3]. Bulk nonlinear KTP crystals ($KTiOPO_4$) are most frequently used for the $1.06 \rightarrow 0.53$ μm conversion [4]. These crystals are characterised by high nonlinear susceptibility of the polarisation interaction of the sf – f type and considerable temperature, spectral and angular widths of the phase matching [4, 5]. A serious drawback of the crystal is high absorption in the blue – green region of the transparency window. In this case, the linear absorption coefficient increases with increasing the probe radiation intensity in the entire transparency range ('grey' losses) and saturates, preserving the saturated value for a long time [6]. This nonlinear phenomenon, called grey tracking, has a threshold decreasing with increasing the fundamental radiation frequency. This threshold is ~ 100 MWcm^{-2} at ~ 0.53 μm for nanosecond pulses and decreases with increasing the pulse duration [6 – 9].

One of the ways to overcome this effect is the heating of the crystal to the temperature above 100 °C [6, 7, 10, 11]. For such temperatures in the KTP crystal, the SHG is possible in the case of angle-uncritical sf – f phase matching along the crystallographic axis *X* with the generation in the green range at a wavelength longer than 0.53 μm [12, 13]. In this case, due to the absence of energy drifts of extraordinary waves, it is possible to use long aperture-unlimited crystals, which is especially expedient at high average and pulsed powers of the converted radiation when tight focusing of light necessary for single short crystal leads to accumulating photochemical changes or to a possible damage of the crystal.

In this paper, to increase the resolution of a polygraphic laser engraving, we studied the possibility of obtaining the green radiation (with the average power of several watts) by the SHG in one and two channels in the KTP crystal from a relatively wideband Yb^{3+} fibre laser and experimentally determined the reasons limiting the maximum second harmonic (SH) power.

2. Experimental

Figure 1 shows the scheme of the experimental setup. As a radiation source, we used a tunable pulsed diode-pumped Yb^{3+} fibre laser consisting of two cascades – a master cascade and an amplifying cascade. Besides the isotropic optical fibre doped with Yb^{3+} ions, master cascade (*1*) included an anisotropic filter with a Faraday mirror and rotator [14] and an acoustooptic *Q* switch providing electronic tuning of the laser wavelength in a pulsed operation regime. Cascade (*4*) consisted of two fibre Yb^{3+} amplifiers.

IR radiation with the numerical aperture NA ~ 0.1 emitted from the end of the output single-mode optical fibre was collimated by gradient lens (*5*) integrated into this fibre into a beam with the waist diameter of about 300 μm, which was placed on the outer end of this lens. Then, the laser radiation was converted by replaceable two-lens objective (*7*) into beams with the waist diameters from 50 to 300 μm, which were placed in the region of the nonlinear crystal. Relatively small waist diameters allowed

B.L. Davydov, A.A. Krylov IRE-Polus Research Association, pl. Vvedenskogo 1, 141120 Fryazino, Moscow region, Russia; e-mail: sokolak@mail.ru

Received 31 June 2006; revision received 9 January 2007
Kvantovaya Elektronika **37** (7) 661 – 668 (2007)
Translated by I.A. Ulitkin

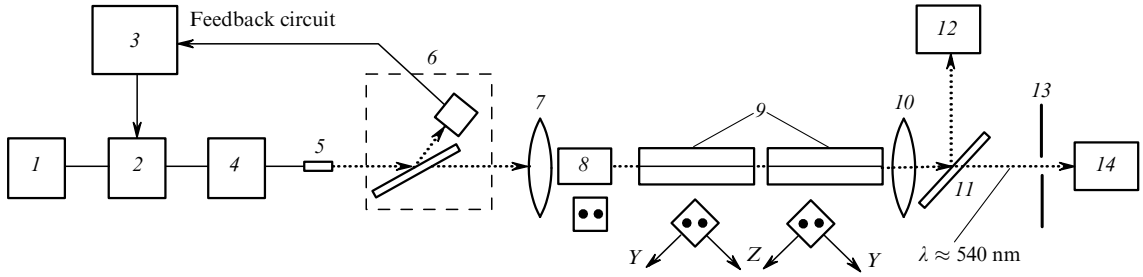

Figure 1. Experimental scheme of the SH generator: (*1*) master pulsed tunable Yb^{3+} fibre laser; (*2*) Billings polarisation controller on two $LiNbO_3$ crystals (2 mm × 3 mm × 24 mm); (*3*) controller processing unit; (4) two-cascade fibre Yb^{3+} amplifier; (*5*) gradient lens integrated into the output optical fibre with a W-shaped refractive index profile, which collimates the laser beam to the waist diameter of 300 μm; (*6*) polarisation-state detector (Brewster plate + silica photodiode); (*7*) two-lens TBF-10 glass objective corrected for spherical aberration; (*8*) calcite parallelepiped polarisation beamsplitter (input beams are shown below); (*9*) KTP crystals (beams as well as orientations of the crystals and their crystallographic axes are shown below); (*10*) quartz long-focus lens; (*11*) dichroic plate separating beams at 1080 and 540 nm; (*12*) Molectron power meter; (*13*) aperture; (*14*) Molectron power meter (at low SH radiation powers – a silica photodiode with a Lambert diffuser in the form of polished quartz plate).

us to obtain SH in each crystal both in one generation channel and in two parallel channels with orthogonal polarisation planes of the fundamental harmonic radiation (Fig. 1). The latter scheme was used to reduce the radiation intensity of the fundamental and second harmonics in the crystal and to decrease the influence of polarisation instability of radiation from the fibre laser by total power of the SH radiation. Because upon focusing, orthogonally polarised SH radiation beams close to the paraxial ones were collected into one common beam, its power was determined as a sum of their powers. The initial radiation of the fundamental harmonic was split by $CaCO_3$ parallelepiped (4 mm × 4 mm × 8 mm) prism beamsplitter (*8*) into two channels with orthogonal polarisation planes and axes separated by ~ 0.8 mm. According to the SHG conditions of the sf–f type, polarisation planes of the fundamental harmonic radiation in the generation channels made ±45° angles with the axes *Y* and *Z* of KTP crystals. To control the polarisation of the output laser radiation between master cascade (*1*) and amplifying cascade (*4*), Billings polarisation controller (*2*) on two electrooptical $LiNbO_3$ crystals, which was integrated into the isotropic optical fibres, was used. Two control voltages were generated by processor unit (*3*). The program of the processor, when a signal from detector (*6*) was fed to it, provided its minimisation (in the ideal case, its zeroing) by selecting and maintaining these voltages. The detector unit could be rotated smoothly at any angle and be fixed in three angular positions (0, ±45°), which allowed us to change the inclination angle of the polarisation plane of the fundamental harmonic radiation. As a result, beamsplitter (*8*) could produce one or two beams corresponding to one or two generation channels.

To decrease the influence of nonlinear processes on the spectral width of the fundamental harmonic radiation (first of all, due to self-phase modulation [15]), the output ('high-power') cascade of the amplifier was made of an optical fibre with a W-shaped refractive index profile and the size of the fundamental waveguide mode increased up to 14 μm. As a result, the laser had the following parameters: the tuning range was from 1070 ± 0.1 to 1090 ± 0.1 nm, the average output power was from 27 ± 0.2 to 30 ± 0.2 W, the FWHM duration of bell-shaped pulses was 70 ± 10 ns, the pulse repetition rate was 100 kHz, the Gaussian intensity distribution in the transverse cross section of the beam with the quality parameter $M^2 \approx 1.2$, the ratio of the intensities of orthogonal polarisation components of the output laser radiation (linear polarisation) was 20 dB, the instability of the average output power during 5 hours of continuous operation ($\lambda = 1080$ nm) was 2 %.

Due to the influence of nonlinear processes in optical fibres, the width of the laser radiation spectrum increases with increasing the average output power. Because the parameters of the SH radiation substantially depend on the spectral width of the fundamental harmonic radiation, we studied the dependence of this width on the average fundamental harmonic power (Fig. 2) (the spectra were recorded with an Anritsu MS-9710A spectrum analyser with the 0.07-nm resolution).

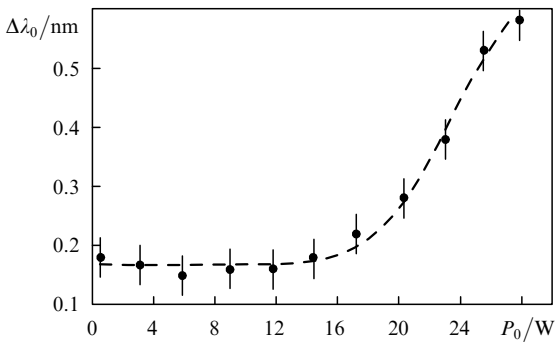

Figure 2. Dependence of the radiation linewidth $\Delta\lambda_0$ of the fundamental harmonic from the Yb^{3+} laser on the average power P_0 for $\lambda_0 =$ 1077.8 nm; vertical lines on the experimental points correspond to the spectral resolution of the Anritsu Ms-9710A spectrum analyser.

The KTP crystals under study (manufactured at the Polus Research and Development Institute) were oriented as shown in Fig. 1 and represented elongated parallelepipeds with the dimensions 19 mm × 5 mm × 5 mm and 30 mm× 3 mm × 3 mm along the axes *X*, *Y* and *Z*, respectively. The end facets of the crystals had AR coatings at 1080 and 540 nm. Both single crystals and pairs of identical crystals separated by ~ 0.5 mm were used in the measurements. The crystals were placed in small-size cylindrical ovens with closed quartz windows. The heaters were made of metal wire wound on ceramic cylinders (the temperature was regulated from the room temperature to 200 °C with the accuracy of ±0.1 °C). To improve the thermal contact with the internal

surface of the cylinder, the crystals were tightly wrapped into the aluminium foil. The electronic control system allowed us to maintain the necessary temperature, which was measured with a thermocouple fixed on one of the crystal sides. The ovens were placed on a translation-angular alignment stage (the accuracy of angle reading was 1 mrad). The SH power was maximised by selecting either the optimal temperature of the oven heating at the given wavelength of the fundamental harmonic or the optimal wavelength of the fundamental harmonic at a fixed temperature, which was detected with the thermocouple, or angular and translational alignments of the crystal.

The radiation of the fundamental and second harmonics was separated with dichroic plate (*11*). Two (or one) orthogonally polarised SH beams were focused by quartz objective (*10*) on the receiving site of diameter 4 mm of Molectron power meter (*14*) into a spot of diameter ~ 2 mm. For relative measurements of the low SH powers, we used a silica FD-3 photodiode with a Lambert diffuser in the form of a quartz plate polished from both sides. The power of the fundamental harmonic radiation reflected from dichroic plate (*11*) was controlled with Molectron power meter (*12*).

3. Results

Figure 3 shows the experimental, nearly linear dependence of the phase-matching wavelength on the temperature of the KTP crystal with a constant angular orientation, which was recorded at an average 1-W power of the fundamental harmonic in one SHG channel (the power of the SH radiation was maximised by selecting the optimal angular orientation of the crystal, which then remained constant). Because we did not have a possibility to determine accurately the orientation of the X axis in our crystals with respect to the direction of radiation propagation, the angular phase-matching direction was near this axis of the KTP crystal and we failed to realised the phase matching exactly in the direction of the crystallographic axis X. Because of this and the difference in properties of the crystals used in the experiment, the obtained phase-matching temperatures do not coincide with the results of paper [13] in which the phase matching exactly in the direction of the X axis at 1079.6 nm was observed at temperature 54 °C.

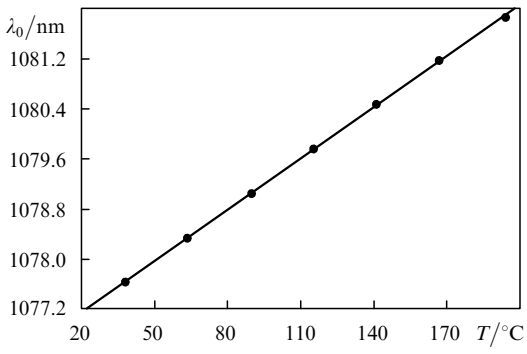

Figure 3. Temperature dependence of the wavelength λ_0 of the sf–f phase matching near the X axis of the KTP crystal for $P_0 = 1$ W, $\Delta\lambda_0 = 0.18$ nm, the waist diameter of the fundamental harmonic beam $2w_0 = 300$ μm and crystal length $L = 30$ mm.

The slope of the straight line was $\sim 27 \times 10^{-3}$ nm deg^{-1}, which agrees with data from paper [16]. Therefore, in the wavelength range from 1077 to 1082 nm even relatively rough heating of the crystal provides fine tuning to the phase matching for the specified wavelength of the fundamental harmonic radiation and angular orientation of the crystal (a change in temperature $\Delta T = \pm 1^\circ$ corresponds to a change in the wavelength $\Delta\lambda = \pm 0.03$ nm).

Figures 4, 5 and 6 show the angular, temperature and spectral dependences of the average output SH power, which were measured at the average ~ 1.5-W power of the fundamental harmonic radiation in one SHG channel in a single 30-mm-long KTP crystal (in this case, the SHG efficiency did not exceed 5 %). Table 1 presents the widths of tuning characteristics of the SH generator calculated by these curves by the angle, wavelength and temperature for the $1080 \rightarrow 540$ nm conversion. In this case, the 'flat' dependence in Fig. 4 corresponds to the case of angle-uncritical phase matching, while the dependence in Figs 5 and 6 correspond to the wavelength- and temperature-critical phase matching [17]. Table 1 also presents the estimates of the sf–f phase-matching widths noncritical over angles θ and φ along the X axis, which were calculated in the approximation of plane monochromatic waves and specified field of the fundamental harmonic by using expressions (1) – (4) taken from paper [5] (the Sellmeier formulas and temperature data for the KTP crystal were borrowed from paper [18], the angular phase-matching width was calculated inside the crystal):

$$2\Delta\varphi = 2\left\{\frac{0.886}{L}\left|\frac{n_Y(\lambda)}{\lambda}\left[1-\left(\frac{n_Y(\lambda)}{n_Z(\lambda)}\right)^2\right]\right.\right.$$
$$\left.\left. - \frac{n_Y(\lambda/2)}{\lambda/2}\left[1-\left(\frac{n_Y(\lambda/2)}{n_Z(\lambda/2)}\right)^2\right]\right|^{-1}\right\}^{1/2}, \quad (1)$$

$$2\Delta\theta = 2\left\{0.886\lambda\left[Ln_Z(\lambda)\left|1-\left(\frac{n_Z(\lambda)}{n_Y(\lambda)}\right)^2\right|\right]^{-1}\right\}^{1/2}, \quad (2)$$

$$2\Delta T = \frac{0.886}{L}\left|\frac{\partial n_Z(\lambda)}{\partial T}+\frac{\partial n_Y(\lambda)}{\partial T}-2\frac{\partial n_Y(\lambda/2)}{\partial T}\right|^{-1}, \quad (3)$$

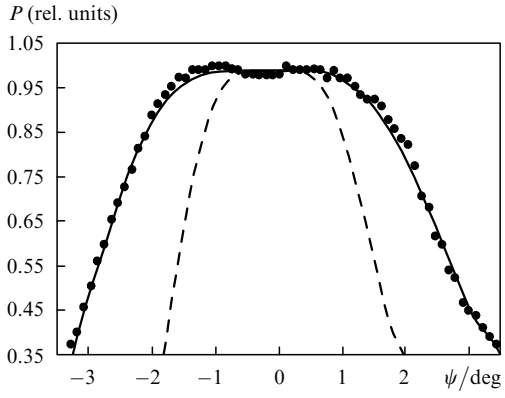

Figure 4. Dependence of the normalised average SH power P on the rotation angle ψ of the KTP crystal in the plane making the 45° angle with the axes Y and Z for $2w_0 = 300$ μm, $T_0 = 124$ °C, $\lambda_0 = 1080$ nm, $\Delta\lambda_0 \approx 0.18$ nm, $L = 30$ mm; points are experimental results for angles in the air and the dashed curve is the result of calculation by the angles in the crystal.

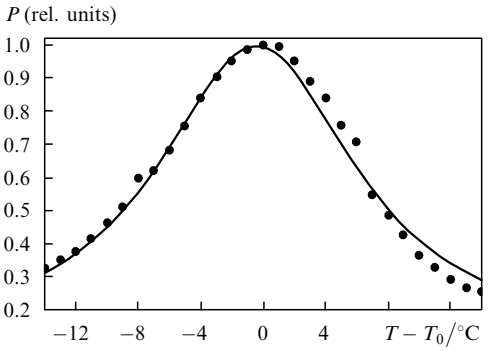

Figure 5. Dependence of the normalised average SH power P on the change in the crystal temperature with respect to the initial temperature $T - T_0$ for $2w_0 = 300$ μm, $T_0 = 65\,^\circ$C, $\lambda_0 = 1078.4$ nm, $\Delta\lambda_0 \approx 0.18$ nm, $L = 30$ mm.

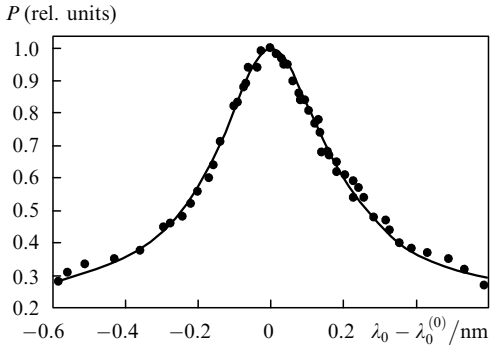

Figure 6. Dependence of the normalised average power P of the SH radiation on the displacement of the central radiation wavelength λ_0 of the fundamental harmonic with respect to the initial one $[\lambda_0^{(0)}]$ for $2w_0 = 300$ μm, $T_0 = 28\,^\circ$C, $\lambda_0^{(0)} = 1077.4$ nm, $\Delta\lambda_0 \approx 0.18$ nm, $L = 30$ mm.

$$2\Delta\lambda = \frac{0.886\lambda}{L}\left|\frac{\partial n_Z(\lambda)}{\partial\lambda} + \frac{\partial n_Y(\lambda)}{\partial\lambda} - 2\frac{\partial n_Y(\lambda/2)}{\partial(\lambda/2)}\right|^{-1}. \qquad (4)$$

Here, L is the crystal length; λ is the radiation wavelength in vacuum; n_Y and n_Z are refractive indices for radiation polarised along the crystal axes Y and Z, respectively.

According to Table 1 all the widths of tuning characteristics significantly exceed the corresponding theoretical values, which is mainly caused by the quality of the fundamental harmonic radiation, namely, the wide spectrum ($\Delta\lambda_0 \approx 0.18$ nm) comparable with the calculated spectral phase-matching width ($2\Delta\lambda \approx 0.1$ nm), the divergence of the fundamental harmonic radiation and the properties of given KTP crystals used in the measurements as well as peculiarities of the experiment itself (in other words, the tuning characteristics of the SH generator represent a convolution of an ideal phase-matching curve with the spatial and frequency Furrier spectrum of the fundamental harmonic radiation).

Table 2 presents the results of additional studies of the influence of spectral and spatial characteristics of the fundamental harmonic radiation on the width of the spectral tuning characteristic of the SH generator in the 19-mm-long KTP crystal ($T_0 = 20\,^\circ$C). One can see that when the spectrum of the fundamental harmonic radiation narrows down and its divergence decreases, the experimental values of the width of the spectral tuning characteristic of the SH generator approach the calculated values, which is quite natural.

Table 1. Widths of tuning characteristics of the SH generator on a single 30-mm-long KTP crystal.

Experiment, calculation	$2\Delta\theta$/deg	$2\Delta\varphi$/deg	$2\Delta T$/K	$2\Delta\lambda$/nm
Experiment: 1080 → 540 nm ($\varphi \approx 0$, $\theta \approx 90^\circ$, $2\Delta\theta_d^{*)} = 0.15^\circ$, $\Delta\lambda_0 \approx 0.18$ nm)	$2\Delta\psi^{**)} = 3.3 \pm 0.1$		16.7 ± 0.2	0.50 ± 0.07
Calculation by (1)–(4): 1078.1 → 539.05 nm ($\varphi = 0$, $\theta = 90^\circ$, $\Delta\lambda_0 \ll 0.1$ nm, $T = 20\,^\circ$C)	1.52	1.41	6.64	0.085

*) $2\Delta\theta_d$ is the divergence of the fundamental harmonic radiation; **) the angular width of the tuning characteristic is denoted by $\Delta\psi$ because the angular dependence of the output average SH power was measured in the plane making the 45° angle between the axes Y and Z of the crystal, which is caused by the experimental conditions

Table 2. Width $2\Delta\lambda$ (nm) of the spectral tuning characteristic of the SH generator for different parameters of the fundamental harmonic radiation.

$2w_0 = 50$ μm, $2\Delta\theta_d = 0.87^\circ$		$2w_0 = 85$ μm, $2\Delta\theta_d = 0.51^\circ$, $\Delta\lambda_0 = 0.14$ nm	Calculation by (4), $\Delta\lambda_0 \ll 0.1$ nm
$\Delta\lambda_0 = 0.20$ nm	$\Delta\lambda_0 = 0.14$ nm		
$0.58 \pm 0.02^{*)}$	$0.48 \pm 0.02^{*)}$	$0.41 \pm 0.01^{*)}$	0.134

*) the error is determined by the accuracy of the approximation of the experimental curve by the Gaussian function.

However, in our case the correctness of the description of nonlinear frequency conversion by the experimental data is confirmed by the fact that the experimental ratio of the spectral width of the tuning characteristic to the temperature one (30×10^{-3} nm deg^{-1}) is close to the slope of the temperature dependence (27×10^{-3} nm deg^{-1}) of the phase-matching wavelength (Fig. 3).

The use of a $CaCO_3$ prism beamsplitter in the SHG scheme (Fig. 1) increased by ~ 20 % the conversion efficiency of the fundamental harmonic radiation with an arbitrary polarisation state in the range of average fundamental harmonic power from 0 to 3 W and for waists with diameters 100 and 150 μm (in this experiment the Billings polarisation controller was not used). Thus, a two-fold decrease in the radiation intensity of the fundamental harmonic with an arbitrary polarisation state in each channel in the two-channel SHG regime leads to an increase in the conversion efficiency to the SH. This regime can be used to optimise the generation of the SH radiation with an arbitrary polarisation state (for any polarisation of the fundamental harmonic radiation, the power of the second harmonic will not decrease lower than a certain value), which is especially effective when a fibre laser serves as a radiation source.

Figure 7 shows the dependences of the SHG efficiency on the average fundamental harmonic power under different experimental conditions. The SH power in each point was maximised by tuning the crystal temperature at constant fundamental harmonic wavelength and angular orientation of crystals. Note the differences in shapes of curves (*3*) and (*4*) corresponding to crystals of equal length and equal sizes of waists of fundamental harmonic beams but substantially different crystal temperatures. The maxima of the efficiencies in curves (*2–5*) corresponded to the fundamental

harmonic powers for which the generation channel was damaged near the output facet of the crystal and a characteristic small-bubble trek was produced, the last crystal being damaged in the tandem of two. Thus, the effect of the channel damage had a threshold character; in this case the threshold SH power decreased with increasing the initial crystal temperature. The behaviour of curves (*1*), (*3*) and (*6*) in Fig. 7 (achievement of the maximum and saturation of the conversion efficiency for a certain fundamental harmonic power) agrees with the theoretical [19–21] and experimental [9] results, in which the effect of the thermal self-action of the fundamental and second harmonic radiation during the SHG in a quasi-stationary regime and in a pulsed regime with pulse durations of the order of hundreds of microseconds was considered. Due to thermal self-actions of the fundamental and second harmonic radiation, the increase in the conversion efficiency to the SH with increasing the fundamental harmonic power terminates by achieving the maximum whose position depends on the crystal sizes, the Gaussian beam waist size of the fundamental harmonic, phase mismatching on the beam axis and the linear absorption coefficient of the crystal. In this case, the maximum integral SHG efficiency is realised for a non-zero phase mismatching on the generation-channel axis [20, 21], which, in turn, leads to the distortion of the spatial intensity distribution of the SH radiation. The Gaussian distribution is transformed into axially symmetric ring distribution, the depth of the dip on the beam axis increasing with increasing the integral SH power. Thus, for curve (*1*) in Fig. 7 the characteristic average SH power, for which the SH radiation beam was substantially distorted, was 1.5 W and for 3-W power, the intensity on the beam axis decreased nearly to the zero level (Fig. 8, the spatial distribution of the radiation intensity was scanned by a multimode fibre with the core diameter 110 μm, the output signal of which was fed to the FD-3 silica photodiode).

Figures 9 and 10 also confirm the fact of thermal self-action during the SHG. These figures show the change in the optimal crystal temperature with increasing the SH power at a specified wavelength of the fundamental harmonic radiation and a change in the optimal wavelength of the fundamental harmonic radiation with increasing the SH power at a constant temperature of the crystal side. In both cases the nonuniform self-heating of the generation channel in the transverse cross section of the crystal causes nonuniform wavelength temperature-dependent mismatching, for partial compensation of which and for maximisation of the SH power one should either decrease the crystal temperature (Fig. 9) or, based on Fig. 3, increase the wavelength of the fundamental harmonic radiation (Fig. 10) [19, 20].

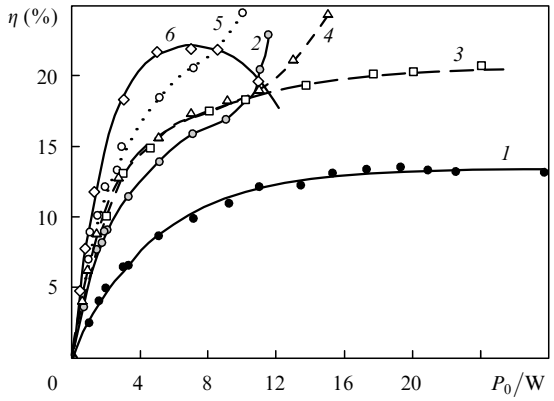

Figure 7. Dependences of the SHG efficiency η on P_0 in a single generation channel for $2w_0 = 300$ μm, $L = 30$ mm, $T_0 = 180\,^\circ$C, $\lambda_0 = 1081.5$ nm (*1*); $2w_0 = 300$ μm, $L = 30$ mm, two tandem crystals are oriented according to Fig. 1 and have the same temperature $T_0 = 180\,^\circ$C, $\lambda_0 = 1081.5$ nm (*2*); $2w_0 = 150$ μm, $L = 19$ mm, $T_0 = 40\,^\circ$C, $\lambda_0 = 1077.7$ nm (*3*); $2w_0 = 150$ μm, $L = 19$ mm, $T_0 = 180\,^\circ$C, $\lambda_0 = 1081.5$ nm (*4*); $2w_0 = 150$ μm, $L = 30$ mm, $T_0 = 180\,^\circ$C, $\lambda_0 = 1081.5$ nm (*5*); $2w_0 = 100$ μm, $L = 19$ mm, $T_0 = 40\,^\circ$C, $\lambda_0 = 1077.7$ nm (*6*). In all the cases the beam waist of the fundamental harmonic is in the centre of the first crystal.

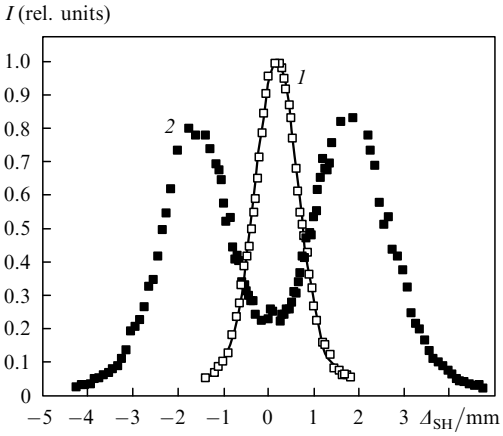

Figure 8. Dependences of the intensity I on the displacement of the scanning optical fibre with respect to the centre of the generation channel of the SH radiation Δ_{SH} for $P = 0.1$ (*1*) and 3.3 W (*2*) in one SH generation channel for $L = 30$ mm, $2w_0 = 300$ μm (the waist is in the crystal centre), $\lambda_0 = 1081.7$ nm, $T_0 \approx 185\,^\circ$C; points are experiment and the curve is Gaussian interpolation.

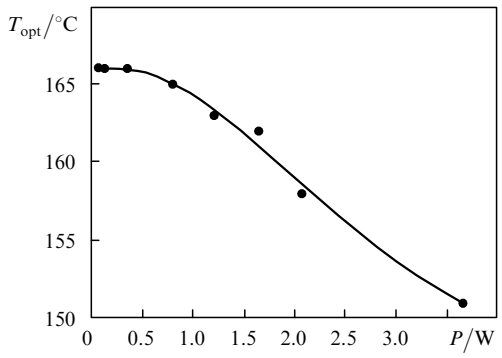

Figure 9. Change in the optimal temperature T_{opt} of the KTP crystal corresponding to the maximum average SH power P for a fixed radiation wavelength of the fundamental harmonic $\lambda_0 \approx 1081$ nm, $L = 19$ mm, $2w_0 = 150$ μm; one SH generation channel.

The further increase in the radiation power of the fundamental and second harmonics leads to the fact that thermal focusing of radiation of these harmonics at the crystal length takes effect, which finally results in the damage of the generation channel near the output facet of the nonlinear crystal [9]. Figure 11, which presents a significant broadening of the fundamental harmonic beam (in the Fraunhoffer region) during the SHG, indicates the presence of focusing and shows that at the initial stage

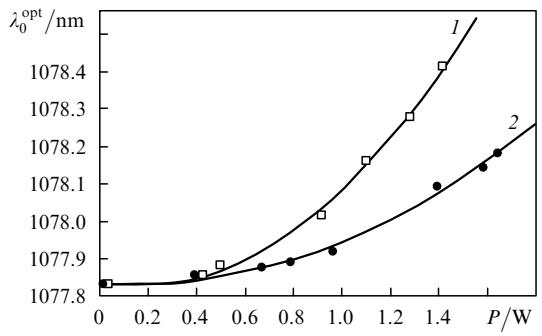

Figure 10. Change in the optimal radiation wavelength λ_0^{opt} of the fundamental harmonic upon sf–f matching near the X axis of the KTP crystal with increasing the average SH power at the fixed crystal temperature $T_0 = 46\,^{\circ}C$ for $2w_0 = 60$ (*1*) and 100 μm (*2*); $L = 19$ mm, one SH generation channel, waists are in the crystal centre.

(away from the damage threshold of the generation channel) the heating of the generation channels is obviously caused by absorption of only SH radiation (because even the maximum radiation intensity of the fundamental harmonic in this case does not exceed 5 MW cm^{-2}, the appearance of grey tracking due to nonlinear effects of two-photon absorption is hardly possible). Besides thermal self-actions during the SHG, another factor favouring the saturation and decrease in the conversion efficiency to the SH is the broadening of the radiation spectrum of the fundamental harmonic with increasing its power. It is these two factors that determine mainly the behaviour of the curves of the conversion efficiency in Fig. 7.

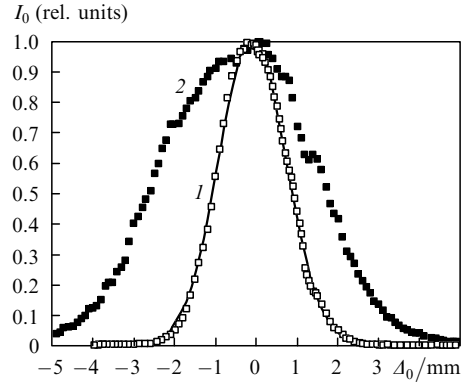

Figure 11. Dependence of the radiation intensity I_0 of the fundamental harmonic in the far field on the displacement Δ_0 of the scanning optical fibre with respect to the centre of the generation channel in the absence of phase matching and during the generation of intense SH radiation under phase-matching conditions; (*1*) radiation power of the fundamental harmonic $P_0 = 24.5$ W; $P = 0$, $\lambda_0 \approx 1078.2$ nm, $T_0 = 174\,^{\circ}C$, one SH generation channel, $2w_0 = 300$ μm, $L = 30$ mm, phase matching is absent, solid curve is the Gaussian interpolation of the intensity distribution in the transverse cross section of the beam; (*2*) $P_0 = 21.3$ W; $P = 3$ W, $\lambda_0 \approx 1081.7$ nm, $T_0 \approx 185\,^{\circ}C$, phase matching is achieved and thermal focusing starts.

Table 3 presents the experimental values of threshold SH powers after the achievement of which the generation channel is damaged due to thermal self-focusing.

The decrease in the threshold power of the SH radiation with increasing the temperature is caused, in our opinion, by the increase in the influence of a thermal lens at the same

Table 3. The threshold SH power at which the generation channel is damaged.

Experimental conditions	P_{th}/W
$2w_0 = 300$ μm, $T_0 \approx 180\,^{\circ}C$, two crystals, $L = 30$ mm	2.3 ± 0.1*)
$2w_0 = 150$ μm, $T_0 \approx 180\,^{\circ}C$, one crystal, $L = 30$ mm	2.1 ± 0.1
$2w_0 = 150$ μm, $T_0 \approx 180\,^{\circ}C$, one crystal, $L = 19$ mm	3.7 ± 0.1
$2w_0 = 150$ μm, $T_0 \approx 40\,^{\circ}C$, one crystal, $L = 19$ mm	5.1 ± 0.2
$2w_0 = 100$ μm, $T_0 \approx 40\,^{\circ}C$, one crystal, $L = 19$ mm	2.2 ± 0.1

*) the generation channel was damaged near the output facet of the last crystal, the beam waist of the fundamental harmonic in all the cases was in the centre of the first crystal.

average SH power, i.e. with the increase in the temperature difference on the axis of the generation channel and the crystal side. The latter circumstance can be caused by a decrease in the thermal conductivity in the KTP crystal with increasing temperature. It is known [22] that the thermal conductivity of dielectrics determined by nonlinear processes of phonon scattering in the crystal (or to be more exact, anharmonic character of the lattice oscillations at high temperatures) depends on the absolute temperature according to the $T^{-\gamma}$ law, where γ takes values from 1 to 2. However, we failed to find data on the temperature dependence of the KTP crystal, hence, we restrict ourselves to the estimate of how much the thermal conductivity decreases with increasing temperature.

In the stationary regime, the distance calculated from the position of the Gaussian beam waist, at which it is focused due to thermal focusing, is written in the form [23]

$$R_T = w_0 \left[n_0 \left(\frac{dn}{dT} \Delta T \right)^{-1} \right]^{1/2} \tag{5}$$

in the absence of aberrations. Here, n_0 is the unperturbed refractive index of the medium at the lasing wavelength; ΔT is the temperature difference in the beam centre and at its periphery. For the constant temperature of the side surface of the medium [20, 21]

$$\Delta T \approx C_0 \frac{\alpha P_{in}}{\kappa}, \tag{6}$$

where α is the linear absorption coefficient; P_{in} is the radiation power at the input to the medium; κ is the thermal conductivity; C_0 is a constant depending on the ratio of the transverse size of the medium to the beam-waist radius. In this case the power of the initial Gaussian beam with the waist radius w_0 should be higher than critical and determined by the expression

$$P_{cr} = P_1 \left[1 - \exp\left(-\frac{\alpha \pi w_0^2}{\lambda} \right) \right]^{-1}, \tag{7}$$

where

$$P_1 = \lambda \kappa \left(\frac{dn}{dT} \right)^{-1}.$$

It follows from (6) that if the crystal absorbs only the SH radiation,

$$\Delta T \approx CP. \tag{8}$$

Here, C is a constant depending on the absorption and

thermal conductivity coefficients, the beam radius, crystal sizes and temperature. One can see from (5) and (6) that R_T depends on the ratio $(\kappa/P)^{1/2}$. By using this fact and data from Table 3 (third and fourth lines) and by assuming the equality of the R_T values in these cases (which is quite reasonable because damage treks of the generation channels were located at nearly equal distances from the output facet of the crystal, and, hence, from the position of the beam waist of the fundamental harmonic), we estimate the change in the thermal conductivity of the KTP crystal with increasing temperature as

$$\frac{\kappa(180\,^\circ\mathrm{C})}{\kappa(40\,^\circ\mathrm{C})} \approx \frac{P(180\,^\circ\mathrm{C})}{P(40\,^\circ\mathrm{C})} = 0.73,$$

i.e. the thermal conductivity decreases approximately by 30 %.

The dependence in Fig. 9 allows us to estimate the constant C by the angular coefficient of the slope of the straight line, which approximates the dependence of the optimal crystal temperature on the SH radiation power for a specified radiation wavelength of the fundamental harmonic (we assume that the change in the temperature is equal to some temperature averaged over its length on the axis of the generation channel and on the crystal side): $C(170\,^\circ\mathrm{C}) = 4.7 \pm 0.3$ K W^{-1}. In this case, relation (8) is valid which is confirmed by the dependence in Fig. 9 for average SH powers exceeding 0.5 W.

By using (6) and (8) we can estimate the linear absorption coefficient at the SH wavelength for temperature $\sim 170\,^\circ$C by the expression

$$\alpha \approx C(170\,^\circ\mathrm{C})\kappa, \tag{9}$$

which yields $\alpha = (10.0 \pm 0.6) \times 10^{-2}$ cm^{-1} ($\kappa = (3 \times 10^{-2}) \times 0.73$ W cm^{-1} K^{-1} [4, 5]). The smaller the diameter of the fundamental harmonic beam, the worse the estimate of α by expression (9) (in fact, it suits the collimated beam upon its small distortions due to thermal self-action). In addition the constant C determined above roughly reflects the real difference in temperatures on the axis of the generation channel and crystal side. Expression (10) from papers [20, 21] gives a more exact estimate, this expression being derived under the following assumption: absorption coefficients of the crystal at wavelengths of the fundamental and second harmonics are equal, the collimated beam of the fundamental harmonic is Gaussian, distortions of the fundamental harmonic beam due to the thermal self-actions are low and the temperature of the crystal side is specified. In this case,

$$\alpha \approx 2\pi C\kappa \left[\ln 2 + 2\ln\left(\frac{r}{w_0}\right) + 0.577\right]^{-1}$$

$$= (7.8 \pm 0.5) \times 10^{-2}\ \mathrm{cm}^{-1}, \tag{10}$$

where $r = 2.5$ mm is a distance from the crystal side to the beam axis. The estimate obtained by using expression (10) exceeds the linear absorption coefficient measured experimentally in the KTP crystal by 2.5 times [6] (3.0×10^{-2} cm^{-1} is a typical value of the coefficient for this crystal at 530 – 540 nm), hence, we can assume that it is the enhanced linear absorption of crystals at the SH wavelength that is the main reason of appearance of thermal self-actions during the SHG with the following damage of the generation channel. This means that when the radiation intensities of the fundamental harmonic in the crystal are much lower than the threshold of the appearance of grey tracking (in our case, below 20 MW cm^{-2}), it is high linear absorption at the SH radiation wavelength in the KTP crystal that is one of the main problems for obtaining high average SH powers in it.

Figure 12 demonstrates the results of the experiment aimed at obtaining stable maximum SH power without the degradation of the crystal in time. For this purpose, the polarisation plane of the SH radiation was placed by controller (*2*) so that the $CaCO_3$ prism beamsplitter produced two generation channels with equal powers of the fundamental harmonic radiation in each channel. In this case, the waist diameters in the generation channels were 100 μm. As a result, stable generation was obtained both in a single crystal and two tandem crystals [21] (in this case, the waist was in the centre of the first crystal and the second crystal generated SH from the diverging fundamental harmonic radiation). The average SH power was maximised by tuning the crystal temperature at the constant radiation wavelength of the fundamental harmonic and angular orientation of the crystal. The conversion efficiency of ~ 29 % was obtained in two crystals. In this case, this value was achieved for the pump power of ~ 7 W and next changed slightly, which is caused by the influence of the radiation spectrum of the fundamental harmonic broadening with increasing the power and, as was stated above, by the effect of thermal self-actions during the SHG. When the average pump power was increased to ~ 14 W, the total SH power was ~ 4 W (approximately 2 W in each channel) and was nearly constant within 5 hours without any noticeable degradation [the last point of curve (*2*) in Fig. 12]. In this case the oscillations of the average SH power within the given time were ±5 %, while the oscillations of the average fundamental harmonic power were ±2 %.

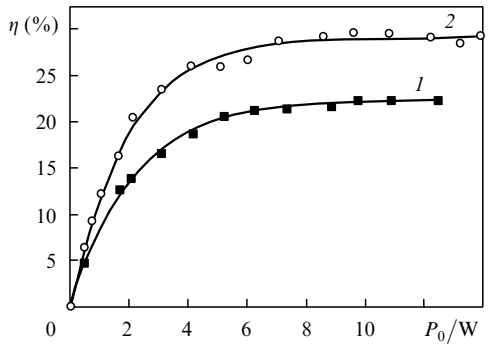

Figure 12. Dependences of the SHG efficiency η in the two-channel generation scheme on the average radiation power P_0 of the fundamental harmonic for $2w_0 = 100$ μm, single crystal (waist is in the crystal centre), $L = 19$ mm. $T_0 = 40\,^\circ$C, $\lambda_0 = 1077.7$ nm (*1*) and for $2w_0 = 100$ μm, two crystals (waist is in the centre of the first crystal), $L = 19$ mm. $T_0 = 40\,^\circ$C, $\lambda_0 = 1077.7$ nm (*2*).

4. Conclusions

(i) The temperature dependence of the phase-matching wavelength as well as the angular, temperature and spectral tuning characteristics of the SH generator in a bulk KTP crystal have been studied upon sf – f phase matching near

the crystallographic axis X, where the tunable pulsed Yb^{3+} fibre laser served as a source of the fundamental harmonic radiation. The widths of tuning characteristics turned to be substantially larger than the corresponding widths of the sf–f phase matching uncritical over the angles θ and φ along the crystallographic axis X, which is related mainly to the quality of the fundamental harmonic radiation (namely, to the wide spectrum comparable with the spectral matching width and angular divergence comparable with the angular phase-matching widths) as well to the quality of the KTP crystals under study.

(ii) The experiments have shown that the average SH radiation powers of several watts and rather high conversion efficiencies to the SH in the KTP crystal can be quite achievable even at a high linear absorption coefficient at the SH wavelength (the experimental estimate of which is $\sim 10^{-1}$ cm^{-1}) without degradation in time. In this case, average fundamental harmonic powers can exceed the crystal damage threshold due to thermal self-focusing appearing because of a high linear absorption of the SH radiation. The decrease in the average radiation power in a single crystal can be achieved by using a two-channel SH generator and summing the SH powers in several crystals. In addition, the two-channel scheme provides intense SH radiation even in the case of arbitrary polarisation state of the fundamental harmonic, which is especially important if a fibre laser serves as a radiation source.

(iii) By using two KTP crystals in a two-channel SH generator, stable total 4-W SH power has been achieved for the ~ 29 % conversion efficiency to the second harmonic. In this case the oscillations of the average SH power within 5 hours of continuous operation were ± 5 %, while the oscillations of the average fundamental harmonic power were ± 2 %.

References

1. http://www.ipgphotonics.com/
2. Avdokhin A.V., Gapontsev V.P., Vyatkin M.Y., Yagodkin R.I., Dronov A.G., Popov S.V., Taylor R. *20-th Anniversary Conf. on Advanced Solid-State Photonics* (Vien, Austria, 2005, MB20).
3. Vyatkin M.Y., Yagodkin R.I., Dronov A.G., Avdokhin A.V., Gapontsev V.P. *3rd Intern. Symp. on High-Power Fiber Lasers and their Applications* (St. Petersburg, Russia, 2006, HPFL-5).
4. Bierlein J.D., Vanherzeele H. *J. Opt. Soc. Am. B*, **6**, 622 (1989).
5. Dmitriev V.G. et al. *Handbook of Nonlinear Optical Crystals* (New York: Springer, 1995).
6. Boulanger B. et al. *IEEE J. Quantum Electron.*, **35** (3), 281 (1999).
7. Jacco J.C. et al. *Opt. Lett.*, **16** (17), 1307 (1991).
8. Boulanger B. et al. *Appl. Phys. Lett.*, **65** (19), 2401 (1994).
9. Favre S., Sidler T.C., Salathe R.-P. *IEEE J. Quantum Eletron.*, **39** (6), 733 (2003).
10. Angert N.B. *Kvantovaya Elektron.*, **18** (4), 470 (1991) [*Sov. J. Quantum Electron.*, **21** (4), 426 (1991)].
11. Martin M.J. et al. *J. Appl. Phys.*, **76** (11), 7510 (1994).
12. Kato K. *IEEE J. Quantum Electron.*, **27** (5), 1137 (1991).
13. Abrosimov S.A., Grechin S.G., Kochiev S.G., Maklakova N.Yu., Semenenko V.N. *Kvantovaya Elektron.*, **31** (7), 643 (2001) [*Quantum Electron.*, **31** (7), 643 (2001)].
14. Cooper D.G., Dexter J.L., Esman R.D. *IEEE J. Sel. Top. Quantum Electron.*, **1** (1), 14 (1995).
15. Agrawal G.P. *Nonlinear Fiber Optics* (New York: Academic Press, 1989; Moscow: Mir, 1996).
16. Wang S., Pasiskevicius V., Laurell F., Karlsson H. *Opt. Lett.*, **23** (24), 1883 (1998).
17. Grechin S.G., Dmitriev V.G., D'yakov V.A., Pryalkin V.I. *Kvantovaya Elektron.*, **26** (1), 77 (1999) [*Quantum Electron.*, **29** (1), 77 (1999)].
18. Kato K., Takaoka E. *Appl. Opt.*, **41** (24), 5040 (2002).
19. Masakatsu Okada, Shogo Ieiri. *IEEE J. Quantum Eletron.*, **7** (9), 469 (1971).
20. Dmitriev V.G., Konovalov V.A., Shalaev E.A. *Kvantovaya Elektron.*, **2**, 496 (1975) [*Sov. J. Quantum Electron.*, **5**, 282 (1975)].
21. Dmitriev V.G., Tarasov L.V. *Prikladnaya nelineinaya optika* (Applied Nonlinear Optics) (Moscow: Fizmatlit, 2004).
22. Ashcroft N.W., Mermin N.D. *Solid Sate Physics* (New York: Holt, Rinehart and Winston, 1976; Moscow: Mir, 1979).
23. Sukhorukov A.P. *Usp. Fiz. Nauk*, **101** (1), 81 (1970).